Spin Reflection-Induced Field-Free Magnetization Switching in Perpendicularly Magnetized MgO/Pt/Co Heterostructures

Tianli Jin, Gerard Joseph Lim, Han Yin Poh, Shuo Wu, Funan Tan, and Wen Siang Lew*

Cite This: https://doi.org/10.1021/acsami.1c22061

Read Online

ACCESS | Metrics & More | Article Recommendations | Supporting Information

ABSTRACT: Field-free magnetization switching is critical towards practical, integrated spin-orbit torque (SOT)-driven magnetic random-access memory with perpendicular magnetic anisotropy. Our work proposes a technique to modulate the spin reflection and spin density of states within a heavy-metal Pt through interfacing with a dielectric MgO layer. We demonstrate tunability of the effective out-of-plane spin torque acting on the ferromagnetic Co layer, enabling current-induced SOT magnetization switching without the assistance of an external magnetic field. The influence of the MgO layer thickness on effective SOT efficiency shows saturation at 4 nm, while up to 80% of field-free magnetization switching ratio is achieved with the MgO between 5 and 8 nm. We analyze and attribute the complex interaction to spin reflection at the dielectric/heavy metal interface and spin scattering within the dielectric medium due to interfacial electric fields. Further, through substituting the dielectric with Ti or Pt, we confirm that the MgO layer is indeed responsible for the observed field-free magnetization switching mechanism.

KEYWORDS: spin-orbit torque, field-free switching, out-of-plane spin torque, spin reflection, spin-orbit torque efficiency
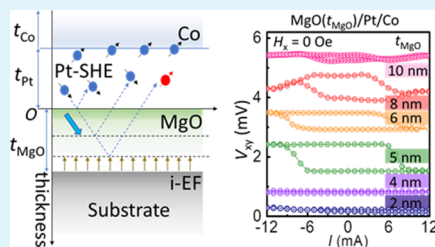
INTRODUCTION

Spin-orbit torque magnetic random-access memory (SOT-MRAM) has been widely slated to be the next generation of MRAM due to its high speed, improved endurance, and better energy efficiency.[1−6] In particular, SOT-MRAM with perpendicular magnetic anisotropy (PMA) boasts excellent thermal stability and scalability.[5−9] However, a collinear in-plane field is generally required to achieve deterministic current-induced SOT magnetization switching in PMA devices, a criterion that challenges the practical integration of SOT-MRAM. Efforts have been made toward the development of field-free SOT switching of PMA devices, such as by breaking the overall symmetry of the system either through its magnetic properties or spin current distribution. For instance, Yu *et al.* demonstrated an external field-free switching technique by utilizing a wedged stack to form a graded anisotropy field in the PMA layer.[10] Subsequent works include the implementation of an in-plane exchange bias field[11] and an in-plane interlayer exchange coupling field.[12] Cai *et al.* introduced a gradient spin-polarized current using a ferroelectric substrate,[13] and Baek *et al.* reported field-free switching using an out-of-plane spin current by modulating the spin orientation via interface spin filtering and precession through the use of an in-plane ferromagnet.[14] Most recently, field-free switching was experimentally demonstrated by out-of-plane spin torque in systems employing low-symmetry crystals.[15] Among these techniques, magnetization switching through an out-of-plane spin torque is most advantageous compared to techniques involving spatial variation and exchange fields as it would not compromise the scalable integration.

Electrons can be polarized when charge current flows through heavy metals (HM).[4,5] Assuming predominantly spin Hall effect (SHE)-induced scattering events experienced by itinerant electrons, oppositely polarized spins accumulate at the lateral interface of the HM. Conventional SOT devices exploit this accumulation of spin for magnetization switching by interfacing the HM with a ferromagnetic (FM) layer, which allows the accumulated spins to cross the HM/FM interface and interact with the FM magnetic moments through angular momentum transfer. Aside from such mechanisms, it is also reported that scattering can occur at seed layer/HM or FM/capping interfaces.[16−21] As such, the spin density of states within an HM layer interfacing with the seed layer can be brought out of balance from purely SHE through spin scattering or spin reflection, which in turn may be used to modulate the spin accumulation at the HM/FM interface. As discussed in previous works on Pt/Co SOT heterostructures, the spin generation along an HM Pt track with a thickness of d can be described by $J_s(d) = J_s(\infty)[1 - \text{sech}(d/\lambda_s)]$ based on the spin drift-diffusion theory, where $J_s(\infty)$ is the spin current at infinite Pt thickness and λ_s is the spin diffusion length.[22−24] Those works mainly dealt with the Pt/Co interface and assumed that no spin current penetrates out of the X/Pt
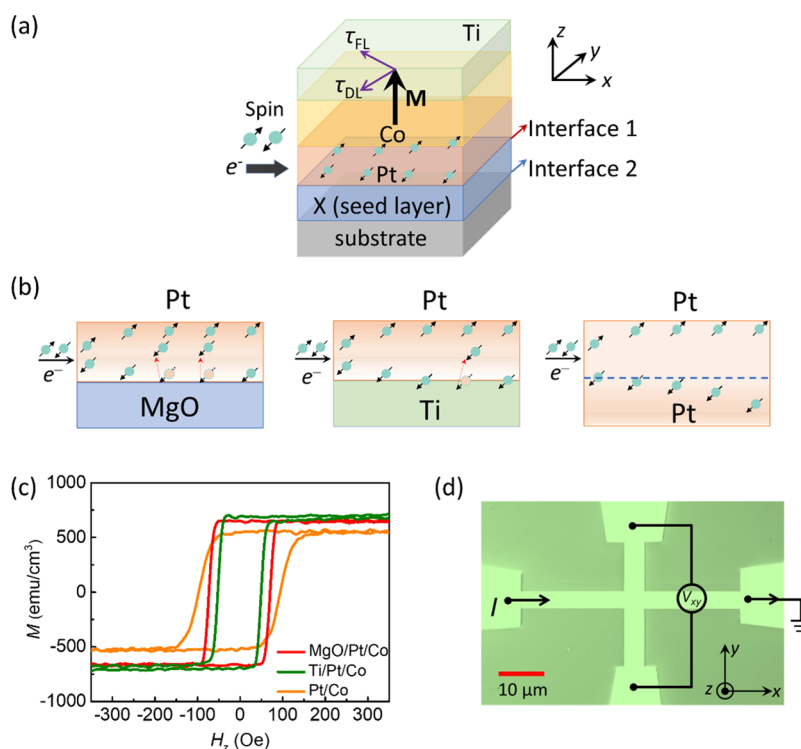
Figure 1. (a) Schematic illustration of the heterostructures with substrate/X/Pt/Co/Ti. The interface of substrate/X and X/Pt is labeled. (b) Depiction of the spin reflection effect from the MgO/Pt and Ti/Pt interface with an arrow and the negligible spin reflection in pure Pt. (c) Hysteresis loops for MgO/Pt/Co, Ti/Pt/Co, and Pt/Co thin film samples. (d) Optical image of the Hall cross device for electric measurements.

interface, where X is the non-FM seed layer interfacing Pt. However, the Rashba-like spin-orbit interaction and spin absorption as well as spin reflection at the X/Pt interface have been seldom discussed. Electrons reflected from the X/Pt interface may realign spin orientations, which will change the spin distribution in the Pt layer.[16,17] Moreover, if X is a dielectric, such as MgO, then an interfacial electric-field is generated due to the difference of electron chemical potentials between the substrate and a dielectric.[25−27] Modifying the thickness of the dielectric layer will allow for the tuning of this interfacial electric field and orientation of the reflected spins.

In this study, we demonstrate the field-free SOT switching in the MgO/Pt/Co heterostructure by modulating the spin reflection and spin density of state within Pt through interfacing with a dielectric MgO layer. Through anomalous Hall voltage loop shift measurements, we determine that the SOT acts as an effective out-of-plane field on the magnetization in the absence of an external magnetic field. By substituting the MgO layer and comparing it with high-conductivity Ti or Pt, we confirm that the MgO is indeed responsible for field-free SOT switching. Moreover, the thickness dependence of MgO reveals an optimal switching ratio of up to 80% between 5 and 8 nm. This work offers the technique to achieve field-free SOT magnetization switching by taking benefits from the spin reflection at the dielectric/HM interface, and it is important to develop SOT-MRAM and spin logic devices in large-scale integration.[28,29] Furthermore, the field-free SOT switching device also has a wide range of non-conventional computing application prospects like brain-inspired computing and deep neural networks.[30,31]

RESULTS AND DISCUSSIONS

Figure 1a illustrates the interfaces of substrate/X and X/Pt by inserting a seed layer X between the substrate and Pt in substrate/X/Pt/Co/Ti heterostructures. When a charge current flows along the Pt layer in the x-direction, spin-up and spin-down electrons are scattered in the opposite directions via the bulk SHE,[32] resulting in a spin current with a polarization p_y aligned along the y-direction. Upon entering the Co layer, the spin current exerts anti-damping torque $\tau_{DL} \approx \mathbf{M} \times (\mathbf{M} \times \mathbf{p}_y)$ and field-like torque $\tau_{FL} \approx \mathbf{M} \times \mathbf{p}_y$ to the magnetic moments of Co.[33] Here, spin scattering at the substrate/X interface is neglected since the spin diffusion length of Pt (1.6−3 nm) is smaller than the thicknesses of the seed layer X and Pt,[4,34] resulting in negligible spin reflected off the substrate/X interface reaching into the Co layer. Therefore, the spin scattering at the X/Pt interface instead of substrate/X is dominant in this particular heterostructure. Figure 1b shows the depiction of the various spin reflection effects from the X/Pt interface with MgO, Ti, and Pt layers. In the case of the heterostructure with X = MgO, spin-down electrons reaching the MgO/Pt interface can penetrate the MgO layer or be reflected back, and afterward it is accumulated at the Pt/Co interface. Furthermore, spin-up and spin-down electrons will be realigned within the Pt layer, which imbalances the spin density of states originally due to bulk SHE.[35,36] The significant spin reflection at the MgO/Pt interface also can be understood from the work function change up to 7 eV of Pt (5.7 eV) and MgO (−1.2 eV) two materials, which will generate an internal electric field pointing to the Pt layer from the MgO layer.[37,38] The existence of the internal electric field at the MgO/Pt interface will interact with the reflected spin, resulting in the spin flip and rotation as well as spin precession. In the case of the heterostructure with X = Ti, down-spin

electrons will be absorbed by the Ti layer due to its high conductivity and less change of work function between Pt and Ti (1.4 eV), resulting in less spin reflection at the Ti/Pt interface. Without a distinct interface for the case of X = Pt, no spin scattering has been considered.

Figure 1c shows the hysteresis loops for substrate/MgO(5)/Pt(3)/Co(1.4)/Ti, substrate/Ti(5)/Pt(3)/Co(1.4)/Ti and substrate/Pt(5)/Co(1.4)/Ti (thickness in nm), which were measured by a vibrating sample magnetometer. The saturation magnetization of these samples is approximately 650 emu/cm^3, and they all display the high remanent magnetization along the out-of-plane H_z direction, indicating the good PMA. For the electrical and optical measurements, Hall cross devices with a width of 5 μm and length of 50 μm were patterned by electron beam lithography and Ar ion milling etching. The optical image is shown in Figure 1d.

The switching behaviors induced by SOT are carried out by sending the pulse current on MgO/Pt/Co Hall cross devices. The pulse width of the current I was fixed at 5 ms. The current amplitude is swept from +15 to −15 mA and then back to +15 mA. The Hall voltage (V_{xy}) was measured after each pulse current by sending a small reading current of 470 μA. The interval of the pulse current is around 2 s. The measurement procedure was illustrated in Figure 2a. The V_{xy} switching
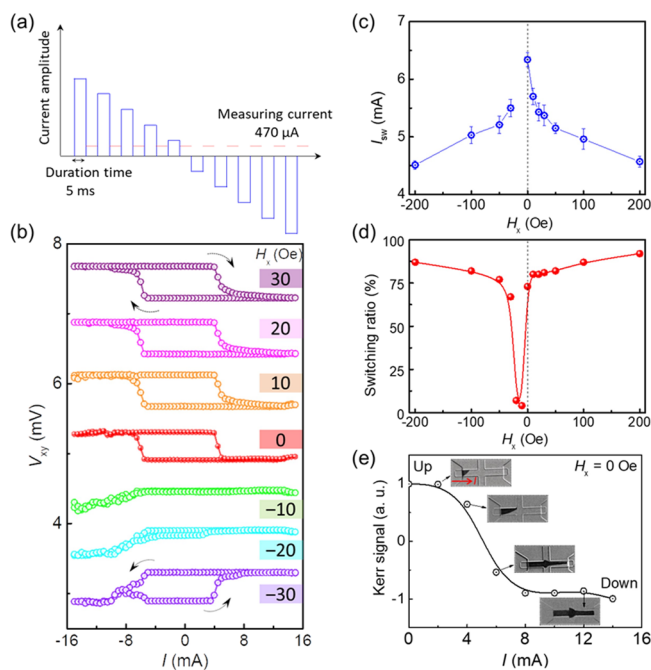

Figure 2. (a) Measurement procedure of the pulse current-induced magnetization switching. (b) Hall voltage V_{xy} with the pulse current I in the MgO/Pt/Co device under different in-plane magnetic fields H_x. (c, d) switching current I_{sw} and switching ratio as a function of H_x for the MgO/Pt/Co sample, respectively. (e) MOKE-normalized signal and domain images with increasing I at H_x = 0 Oe.

curves are shown in Figure 2b with varying the H_x from 30 to −30 Oe. A mostly fully SOT switching loop was observed at H_x = 0 Oe. In addition, almost no switching signal was detected in this sample when H_x = −10 to −20 Oe. These results indicate the existence of an effective internal field that participates in the deterministic SOT switching process. The switching current I_{sw} and the switching ratio as a function of H_x are displayed in Figure 2c,d, respectively. As expected in the

SOT framework, the switching current is reduced with the increasing assistant field H_x, while the switching ratio increases as the magnitude of H_x increases.[3] For Ti/Pt/Co and Pt/Co samples, the magnetization can be fully switched with the assistance of H_x.[39] However, partial switching is demonstrated in the Ti/Pt/Co sample, and the no-switching in the Pt/Co sample is observed at H_x = 0 Oe. The switching curves for Ti/Pt/Co and Pt/Co samples are shown in Supporting Information S3.

To confirm the field-free switching for the MgO/Pt/Co sample and further gain insights into the magnetization switching process, we utilized an MOKE microscope to capture the magnetic domain evolution during switching. The devices were saturated at a large field (H_z = 3000 Oe) to initialize the magnetization to the "up" direction and capture as the reference image. Next, the following images were obtained after each current pulse by subtracting from the reference one. Figure 2e shows the Kerr images and domain states after each pulse current I at the zero field. Pulse currents I with the increasing amplitude were delivered through the wire from left to right in all cases. In the MgO/Pt/Co sample, upon delivery of the increasing current I from 4 mA, a reversed domain first nucleates at the left-top edge, which then expands across the entire strip, resulting in the deterministic full switching.[40] The visualized domain evolution is presented in the inset of Figure 2e, which provides clear evidence for the field-free switching in Figure 2b.

The fully field-free SOT switching was only observed in MgO/Pt/Co, while no indication of field-free switching was observed in the Pt/Co system. The result indicates the significant role of the MgO layer in spin reflection. In this scenario, the spin electrons in the Pt layer with polarization along $+\mathbf{p}_y$ (or $-\mathbf{p}_y$) have been realigned, causing the spin polarization with an out-of-plane component. To confirm the existence and contribution of the out-of-plane spin-orbit torque contribution to the field-free SOT switching in the particular system,[15,41] we carried out the measurements with shifting V_{xy} loops under different DC currents I_{DC}. Figure 3a,b shows the V_{xy} shift loops for MgO/Pt/Co samples at H_x = 0 and H_x = 520 Oe, respectively. The clear V_{xy} loop shift to right and left was observed in the MgO/Pt/Co sample when the I_{DC} is 7 and −7 mA at H_x = 0 Oe. Moreover, the V_{xy} loops become tilted, which is due to the significant Joule heating of high I_{DC}.[42,43] With applied H_x = 520 Oe, the shift field increases and the V_{xy} loops become much narrower. However, the switching loops are merely narrower for Ti/Pt/Co and Pt/Co samples, and no shift has been observed in further increasing the current to 10 mA at H_x = 0 Oe (as shown in Supporting Information S5). The obvious V_{xy}-H loop shift in MgO/Pt/Co clearly confirms the existence of finite SOT without an external field, which is distinguished from the results of Ti/Pt/Co and Pt/Co samples without shift at H_x = 0 Oe. Moreover, with the current smaller than ±6 mA, no obvious shift was detected in MgO/Pt/Co, upon increasing the current to ±7 mA, an abrupt shift was observed, which was similar to the previously reported systems with the presence of the spin current with out-of-plane spin torque component.[15] The shift fields H_{shift} for H_x = 0 and H_x = 520 Oe with I_{DC} have been summarized in Figure 3c. Figure 3d shows the comparable results of H_{shift} for MgO/Pt/Co, Ti/Pt/Co, and Pt/Co samples with H_x = 520 Oe. The linear slope between H_{shift} and I_{DC} can quantitatively manifest the SOT efficiency.[22] The slope of 7.9 ± 0.96 (Oe/mA) was shown in the MgO/Pt/Co sample. For Ti/Pt/Co and Pt/Co
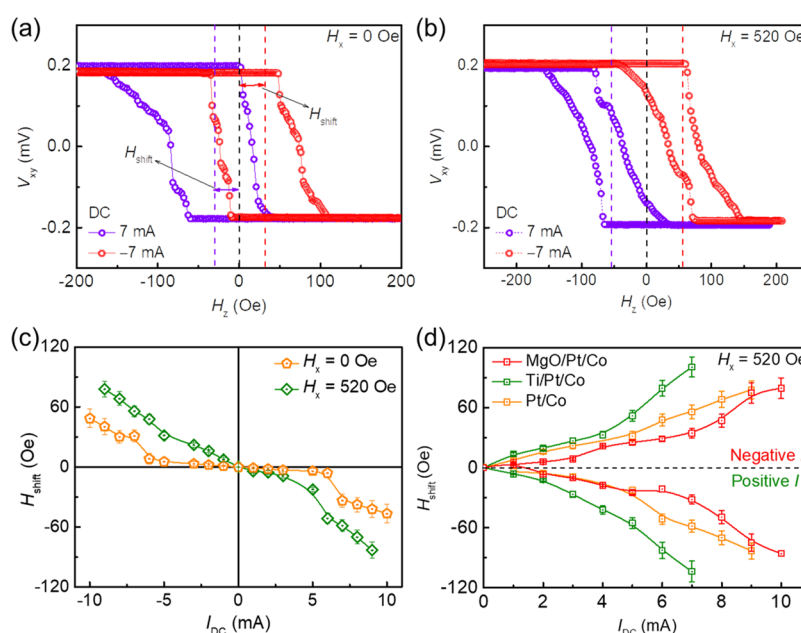
Figure 3. Shift effect of the out-of-plane hysteresis loops under positive DC 7 mA and negative DC −7 mA at an in-plane field: (a) $H_x = 0$ Oe and (b) $H_x = 520$ Oe for the MgO/Pt/Co device. The calculation of the shift field H_{shift} under I_{DC}, defined as the center shifting of the loops, is determined in the inset of (a). (c) Summarized H_{shift} with I_{DC} at $H_x = 0$ and $H_x = 520$ Oe for the MgO/Pt/Co device. (d) H_{shift} with a function of I_{DC} for MgO/Pt/Co, Ti/Pt/Co, and Pt/Co samples at $H_x = 520$ Oe.
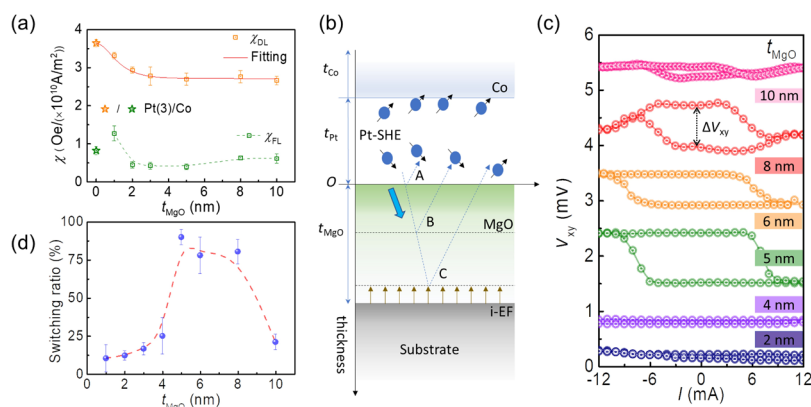
Figure 4. (a) Damping-like field efficiency χ_{DL} and field-like field efficiency χ_{FL} with t_{MgO}. The χ_{DL} and χ_{FL} for the control sample without MgO have been indicated with yellow stars and green stars, respectively. The fitting of χ_{DL} is plotted in the red line. (b) Schematic of spin tunneling and spin relaxation in the MgO layer. The capital A, B, and C indicate the spin reflection mechanics with electrons penetrating into the MgO layer. The interfacial electric-field (i-EF) indicates the electric-field between the Si/SiO$_2$ substrate and the MgO seed layer. (c) Hall voltage V_{xy} with pulse current in the absence of H_x with MgO thickness t_{MgO}. (d) SOT-induced magnetization switching ratio with t_{MgO}.

samples, the slopes are 13.5 ± 1.03 (Oe/mA) and 8.4 ± 0.93 (Oe/mA), respectively. The lower SOT efficiency demonstrated from the loop shift results in the MgO/Pt/Co sample is attributed to the stronger spin reflection from the MgO/Pt interface, resulting in the net spin compensation at the Pt/Co interface. Moreover, we have performed harmonic measurements by sweeping the in-plane magnetic field to further investigate the spin-torque efficiency (as shown in Supporting Information S6).

We, furthermore, tuned the thickness of MgO to investigate the impact on the switching efficiency by performing harmonic measurements and the current-induced switching loops at $H_x = 0$ Oe. Samples with different thicknesses of MgO from 1 to 10 nm all exhibit good PMA, which are denoted as MgO (t_{MgO} nm)/Pt/Co. The differences of Hall voltages ($\Delta V_{xy} = V_U - V_D$) between up and down magnetizations are almost

comparable (as shown in Supporting Information S8). All the MgO/Pt/Co samples display a clear MgO (200) peak, confirmed from X-ray diffraction (XRD) scanning, which indicates a good crystalline quality of MgO. However, a faint peak still can be observed at MgO (111) for the MgO/Pt/Co sample with $t_{MgO} = 1$ nm, which indicates that 1 nm is too thin for MgO to form a good single crystalline (as shown in Supporting Information S9). Figure 4a shows the results of damping-like (DL) field efficiency χ_{DL} and field-like (FL) field efficiency χ_{FL} extracted from the increment of the DL field and FL field with the current density flowing Pt heavy metal layer, with t_{MgO}. The χ_{DL} is around 3.3 Oe/(10^{10} A/m^2) when $t_{MgO} = 1$ nm, which is almost comparable to the control sample Pt (3 nm)/Co without MgO (indicated with a yellow star).[44,45] With t_{MgO} increasing, χ_{DL} shows a decrease to 2.7 Oe/(10^{10} A/m^2). Meanwhile, the χ_{FL} is enhanced to 1.2 Oe/(10^{10} A/m^2) when

inserting a 1 nm MgO layer (indicated with green-star) due to the Rashba field. χ_{FL} almost remaining to 0.9 Oe/(10^{10} A/m^2) with t_{MgO} above 5 nm. The decreasing of χ_{DL} can be fitted as the function of t_{MgO} in eq 1[46]

$$\chi_{DL} = \chi_{Pt} - \chi_{ref}\left[1 - \text{sech}\left(\frac{t_{MgO}}{\lambda_p}\right)\right] \tag{1}$$

Here, χ_{Pt} is the DL efficiency coming from the 3 nm Pt heavy-metal layer, χ_{ref} is the DL efficiency coming from the spin reflection by inserting the MgO seed layer, and λ_p is the parameter to describe the spin penetration length in MgO. Taking the fitting parameters, λ_p is around 0.9 nm, and the contribution from spin reflection to χ_{DL} is saturated when t_{MgO} is larger than 3.8 nm. Moreover, the saturated contribution of χ_{ref} to DL efficiency is 0.92 Oe/(10^{10} A/m^2) with a ratio of χ_{ref}/χ_{Pt} = 25%, which verifies that the spin reflection from MgO/Pt plays an important role in overall DL efficiency, especially for the thin Pt systems. The SOT efficiency with various t_{MgO} also can be estimated from the shift fields H_{shift} with I_{DC} (as discussed in Supporting Information S10).

Thereafter, we carefully considered the impacts of reflected spin on SOT switching and efficiency. As illustrated in Figure 4b, electrons with a specific spin orientation are reflected from different depths in the MgO layer with various mechanisms (marked by A, B, and C). Besides the direct spin reflection from the MgO/Pt interface (marked as mechanism A), the spin may penetrate into the MgO layer by tunneling.[27] By inserting the MgO layer, the interface between the substrate and Pt will be changed from substrate/Pt to MgO/Pt, resulting in a modulation of the interfacial Rashba field. Furthermore, an interface between the substrate and MgO is formed with an interfacial electric-field (i-EF) region due to the different chemical potentials of the two dielectrics. All those combined effects play a role in modulating the spin transport and SOT efficiency in MgO/Pt/Co heterostructures. By inserting a thin MgO layer, the DL efficiency shows a decrease, while the FL efficiency shows a distinct increase at t_{MgO} = 1 nm. With increasing t_{MgO}, the spin tunneling effect is suppressed with low tunneling probability, resulting in more spin reflection, as marked with mechanism B. Then, the reflected spin with the opposite spin direction partially cancels out the spin accumulation at the Pt/Co interface, causing a reduction of the SOT efficiency. For a thicker MgO layer (with t_{MgO} > 4 nm), which is the depth of the spin tunneling saturation, most spin cannot penetrate further into the MgO layer but reaches the region with the i-EF. The spin will be flipped with a new orientation (as marked with C), and it leads to a modification in the spin density of states in the Pt layer, generating an SOT with an out-of-plane component. While inserting a much thicker MgO layer, the spin cannot reach the i-EF regime, which has a penetrating length of around 3−4 nm. The spin can only be reflected without changing its orientation. Therefore, the DL efficiency is saturated for t_{MgO} > 4 nm, and the field-free magnetization switching has been observed only with t_{MgO} in the range from 5 to 8 nm, as demonstrated in Figure 4c. More details have been discussed in Supporting Information S11.

Figure 4d has summarized the switching ratio, which was extracted from the switching loop, defined as $\Delta V_{xy}/\Delta V_H$. The error bar was obtained by measuring the same device 10 times. In the MgO/Pt/Co samples with t_{MgO} < 5 nm, a low switching ratio of less than 25% was obtained and no deterministic

switching was observed without an external field. The reflected electron spin is relatively limited within a thin MgO layer. Hence, it is insufficient to contribute to the field-free deterministic switching. With the increase in MgO thickness, the switching ratio increases. A higher switching ratio (>80%) has been observed in MgO/Pt/Co samples with t_{MgO} in the range from 5 to 8 nm, indicating that a distinct field-free switching can be obtained in this thickness regime. For the thicker MgO layer, the switching ratio starts to decrease. We have confirmed that the bottom interface beneath the heavy metal has significant influences on spin generation and magnetization switching, which have not been fully evaluated in the previous studies. High-efficiency field-free SOT devices may be realized by implementing different types and thicknesses of the seed layers to ensure spin reflection while retaining high SOT efficiency.

■ CONCLUSIONS

Current-induced SOT switching without the assistance of an external magnetic field has been demonstrated in MgO/Pt/Co heterostructures. The magnetization switching can be attributed to the enhanced spin reflection effect from MgO with high resistivity, resulting in an out-of-plane spin torque, which exerts an additional anti-damping on the magnetization of Co for its switching. Moreover, the optimized thickness of MgO is in the range 5−8 nm for field-free magnetization switching. SOT efficiency can be enhanced with a high charge conductivity seed layer to reduce the net spin compensation at the Pt/Co interface. Our work demonstrates a technique for field-free SOT switching and provides an approach to tune the spin generation in both magnitude and orientation.

■ EXPERIMENTAL SECTION

Sample Preparation. In our experiment, the dielectric MgO seed layer was deposited by radio frequency sputtering onto thermally oxidized Si substrates in a vacuum with a base pressure of 5 × 10^{-8} Torr. Subsequently, the samples were transferred to another direct current (DC) sputtering without breaking the vacuum atmosphere followed by Pt (3 nm)/Co (1.4 nm)/Ti (5 nm) deposition with a base pressure of 3 × 10^{-8} Torr. The metal Ti seed layer and Pt (3 nm)/Co (1.4 nm)/Ti (5 nm) stack were grown on Si substrates by DC sputtering. The deposition rates for Pt, Co, Ti, and MgO are 0.127, 0.012, 0.017, and 0.003 nm/s, respectively. Hall cross devices with 5 μm width and 50 μm length were fabricated by electron beam lithography followed by an Ar ion milling, and the electrode consisted of Ti (10 nm)/Cu (80 nm)/Pt (10 nm).

Electrical-Transport Measurements. Current-induced magnetization switching was performed by sending a series of current pulses with 5 ms duration, and after each current pulse, a sensing current of 470 μA was utilized to measure the change in Hall voltage. For the anomalous Hall voltage measurements, current-induced hysteresis loop shift measurements and the effective magnetic fields induced by SOT were demonstrated using a harmonic lock-in technique. The first and second harmonic Hall voltages with an alternating current of 307 Hz were simultaneously measured while sweeping an out-of-plane or in-plane external magnetic fields in different directions.

Magneto-Optic Kerr Effect Microscopy. The MagVision Kerr microscopy system operating in polar mode was used to measure the switching signal and capture the domain images by sending pulse current. The pulse current was sent by using a Keithley 2401 sourcemeter.

ASSOCIATED CONTENT

🅢ⅈ Supporting Information

The Supporting Information is available free of charge at https://pubs.acs.org/doi/10.1021/acsami.1c22061.

Determination of perpendicular magnetic anisotropy (S1), anomalous Hall voltage loops with different currents (S2), current-driven magnetization switching with in-plane field H_x for Ti/Pt/Co and Pt/Co samples (S3), MOKE-normalized signal and domain images with the increasing current amplitude at the zero in-plane field in Ti/Pt/Co and Pt/Co samples (S4), shift effect of the out-of-plane hysteresis loops for Ti/Pt/Co and Pt/Co samples (S5), harmonic Hall voltage measurements (S6), quantitative characterization of the ratio of planar Hall resistance and anomalous Hall resistance (S7), MgO thickness-dependent magnetic properties (S8), X-ray diffraction (XRD) results (S9), out-of-plane hysteresis loops shift for different MgO thickness devices (S10), and spin tunneling and reflection in the MgO layer (S11) (PDF)

AUTHOR INFORMATION

Corresponding Author

Wen Siang Lew − *School of Physical and Mathematical Sciences, Nanyang Technological University, 637371, Singapore;* ⓘ orcid.org/0000-0002-5161-741X; Email: wensiang@ntu.edu.sg

Authors

Tianli Jin − *School of Physical and Mathematical Sciences, Nanyang Technological University, 637371, Singapore;* ⓘ orcid.org/0000-0002-9364-6024

Gerard Joseph Lim − *School of Physical and Mathematical Sciences, Nanyang Technological University, 637371, Singapore;* ⓘ orcid.org/0000-0003-2411-5841

Han Yin Poh − *School of Physical and Mathematical Sciences, Nanyang Technological University, 637371, Singapore*

Shuo Wu − *School of Physical and Mathematical Sciences, Nanyang Technological University, 637371, Singapore*

Funan Tan − *School of Physical and Mathematical Sciences, Nanyang Technological University, 637371, Singapore*

Complete contact information is available at:
https://pubs.acs.org/10.1021/acsami.1c22061

Notes

The authors declare no competing financial interest.

ACKNOWLEDGMENTS

REFERENCES

(1) Han, X.; Wan, C.; Yu, G. Materials, Physics, and Devices of Spin−orbit Torque Effect. *Appl. Phys. Lett.* **2021**, *118*, 120502.

(2) Shao, Q.; Li, P.; Liu, L.; Yang, H.; Fukami, S.; Razavi, A.; Wu, H.; Freimuth, F.; Mokrousov, Y.; Stiles, M. D.; Emori, S.; Hoffmann, A.; Akerman, J.; Roy, K. Roadmap of Spin−Orbit Torques. *IEEE Trans. Magn.* **2021**, *57*, 180401−180439.

(3) Mikuszeit, N.; Boulle, O.; Miron, I. M.; Garello, K.; Gambardella, P.; Gaudin, G.; Buda-Prejbeanu, L. D. Spin-orbit Torque Driven Chiral Magnetization Reversal in Ultrathin Nanostructures. *Phys. Rev. B* **2015**, *92*, 144424.

(4) Liu, L.; Moriyama, T.; Ralph, D. C.; Buhrman, R. A. Spin-torque Ferromagnetic Resonance Induced by the Spin Hall Effect. *Phys. Rev. Lett.* **2011**, *106*, No. 036601.

(5) Pai, C.-F.; Liu, L.; Li, Y.; Tseng, H. W.; Ralph, D. C.; Buhrman, R. A. Spin Transfer Torque Devices Utilizing the Giant Spin Hall Effect of Tungsten. *Appl. Phys. Lett.* **2012**, *101*, 122404.

(6) Miron, I. M.; Garello, K.; Gaudin, G.; Zermatten, P. J.; Costache, M. V.; Auffret, S.; Bandiera, S.; Rodmacq, B.; Schuhl, A.; Gambardella, P. Perpendicular Switching of a Single Ferromagnetic Layer Induced by In-plane Current Injection. *Nature* **2011**, *476*, 189−193.

(7) Ikeda, S.; Miura, K.; Yamamoto, H.; Mizunuma, K.; Gan, H. D.; Endo, M.; Kanai, S.; Hayakawa, J.; Matsukura, F.; Ohno, H. A Perpendicular-anisotropy CoFeB−MgO Magnetic Tunnel Junction. *Nat. Mater.* **2010**, *9*, 721−724.

(8) Peng, S.; Zhu, D.; Li, W.; Wu, H.; Grutter, A. J.; Gilbert, D. A.; Lu, J.; Xiong, D.; Cai, W.; Shafer, P.; Wang, K. L.; Zhao, W. Exchange Bias Switching in an Antiferromagnet/Ferromagnet Bilayer Driven by Spin−orbit Torque. *Nat. Electron.* **2020**, *3*, 757−764.

(9) Li, W.; Peng, S.; Lu, J.; Wu, H.; Li, X.; Xiong, D.; Zhang, Y.; Zhang, Y.; Wang, K. L.; Zhao, W. Experimental Demonstration of Voltage-gated Spin-orbit Torque Switching in an Antiferromagnet/Ferromagnet Structure. *Phys. Rev. B* **2021**, *103*, No. 094436.

(10) Yu, G.; Upadhyaya, P.; Fan, Y.; Alzate, J. G.; Jiang, W.; Wong, K. L.; Takei, S.; Bender, S. A.; Chang, L. T.; Jiang, Y.; Lang, M.; Tang, J.; Wang, Y.; Tserkovnyak, Y.; Amiri, P. K.; Wang, K. L. Switching of Perpendicular Magnetization by Spin-orbit Torques in the Absence of External Magnetic Fields. *Nat. Nanotechnol.* **2014**, *9*, 548−554.

(11) Fukami, S.; Zhang, C.; DuttaGupta, S.; Kurenkov, A.; Ohno, H. Magnetization Switching by Spin-orbit Torque in an Antiferromagnet-ferromagnet Bilayer System. *Nat. Mater.* **2016**, *15*, 535−541.

(12) Kong, W. J.; Wan, C. H.; Wang, X.; Tao, B. S.; Huang, L.; Fang, C.; Guo, C. Y.; Guang, Y.; Irfan, M.; Han, X. F. Spin−orbit Torque Switching in a T-type Magnetic Configuration with Current Orthogonal to Easy Axes. *Nat. Commun.* **2019**, *10*, 233.

(13) Cai, K.; Yang, M.; Ju, H.; Wang, S.; Ji, Y.; Li, B.; Edmonds, K. W.; Sheng, Y.; Zhang, B.; Zhang, N.; Liu, S.; Zheng, H.; Wang, K. Electric Field Control of Deterministic Current-induced Magnetization Switching in a Hybrid Ferromagnetic/Ferroelectric Structure. *Nat. Mater.* **2017**, *16*, 712−716.

(14) Baek, S. C.; Amin, V. P.; Oh, Y. W.; Go, G.; Lee, S. J.; Lee, G. H.; Kim, K. J.; Stiles, M. D.; Park, B. G.; Lee, K. J. Spin Currents and Spin−orbit Torques in Ferromagnetic Trilayers. *Nat. Mater.* **2018**, *17*, 509−513.

(15) Liu, L.; Zhou, C.; Shu, X.; Li, C.; Zhao, T.; Lin, W.; Deng, J.; Xie, Q.; Chen, S.; Zhou, J.; Guo, R.; Wang, H.; Yu, J.; Shi, S.; Yang, P.; Pennycook, S.; Manchon, A.; Chen, J. Symmetry-dependent Field-free Switching of Perpendicular Magnetization. *Nat. Nanotechnol.* **2021**, *16*, 277−282.

(16) Amin, V. P.; Stiles, M. D. Spin Transport at Interfaces with Spin-orbit Coupling: Formalism. *Phys. Rev. B* **2016**, *94*, 104419.

(17) Qiu, X.; Legrand, W.; He, P.; Wu, Y.; Yu, J.; Ramaswamy, R.; Manchon, A.; Yang, H. Enhanced Spin-Orbit Torque via Modulation of Spin Current Absorption. *Phys. Rev. Lett.* **2016**, *117*, 217206.

(18) Bekele, Z. A.; Meng, K.; Miao, J.; Xu, X.; Jiang, Y. Modulated Spin Orbit Torque in Ultrathin Ferromagnetic Layer with Different Capping Layers. *Surf. Coat. Technol.* **2019**, *359*, 354−359.

(19) Ourdani, D.; Roussigné, Y.; Chérif, S. M.; Gabor, M. S.; Belmeguenai, M. Dependence of the Interfacial Dzyaloshinskii-Moriya Interaction, Perpendicular Magnetic Anisotropy, and Damping in Co-based Systems on the Thickness of Pt and Ir Layers. *Phys. Rev. B* **2021**, *104*, 104421.

(20) Hayashi, H.; Asami, A.; Ando, K. Anomalous Hall Effect at a PtOₓ/Co Interface. *Phys. Rev. B* **2019**, *100*, 214415.

(21) Feng, J.; Grimaldi, E.; Avci, C. O.; Baumgartner, M.; Cossu, G.; Rossi, A.; Gambardella, P. Effects of Oxidation of Top and Bottom

Interfaces on the Electric, Magnetic, and Spin-orbit Torque Properties of Pt/Co/AlO$_x$ Trilayers. *Phys. Rev. Appl.* **2020**, *13*, No. 044029.

(22) Chen, Y.; Zhang, Q.; Jia, J.; Zheng, Y.; Wang, Y.; Fan, X.; Cao, J. Tuning Slonczewski-like Torque and Dzyaloshinskii−Moriya Interaction by Inserting a Pt Spacer Layer in Ta/CoFeB/MgO Structures. *Appl. Phys. Lett.* **2018**, *112*, 232402.

(23) Zhu, L.; Ralph, D. C.; Buhrman, R. A. Unveiling the Mechanism of Bulk Spin-Orbit Torques within Chemically Disordered Fe$_x$Pt$_{1-x}$ Single Layers. *Adv. Funct. Mater.* **2021**, *31*, 2103898.

(24) Liu, L.; Lee, O. J.; Gudmundsen, T. J.; Ralph, D. C.; Buhrman, R. A. Current-induced Switching of Perpendicularly Magnetized Magnetic Layers Using Spin Torque From the Spin Hall Effect. *Phys. Rev. Lett.* **2012**, *109*, No. 096602.

(25) De Teresa, J. M.; Barthelemy, A.; Fert, A.; Contour, J. P.; Montaigne, F.; Seneor, P. Role of Metal-oxide Interface in Determining the Spin Polarization of Magnetic Tunnel Junctions. *Science* **1999**, *286*, 507−509.

(26) Zhang, J. Y.; Yang, G.; Wang, S. G.; Liu, Y. W.; Zhao, Z. D.; Wu, Z. L.; Zhang, S. L.; Chen, X.; Feng, C.; Yu, G. H. Effect of MgO/Co Interface and Co/MgO Interface on the Spin Dependent Transport Inperpendicular Co/Pt Multilayers. *J. Appl. Phys.* **2014**, *116*, 163905.

(27) Spiesser, A.; Saito, H.; Yuasa, S.; Jansen, R. Tunnel Spin Polarization of Fe/MgO/Si Contacts Reaching 90% with Increasing MgO Thickness. *Phys. Rev. B* **2019**, *99*, 224427.

(28) Yang, M.; Deng, Y.; Wu, Z.; Cai, K.; Edmonds, K. W.; Li, Y.; Sheng, Y.; Wang, S.; Cui, Y.; Luo, J.; Ji, Y. Spin Logic Devices via Electric Field Controlled Magnetization Reversal by Spin-orbit Torque. *IEEE Electron Device Lett.* **2019**, *40*, 1554−1557.

(29) Luo, Z.; Hrabec, A.; Dao, T. P.; Sala, G.; Finizio, S.; Feng, J.; Mayr, S.; Raabe, J.; Gambardella, P.; Heyderman, L. J. Current-driven Magnetic Domain-wall Logic. *Nature* **2020**, *579*, 214−218.

(30) Vincent, A. F.; Larroque, J.; Locatelli, N.; Romdhane, N. B.; Bichler, O.; Gamrat, C.; Zhao, W. S.; Klein, J. O.; Galdin-Retailleau, S.; Querlioz, D. Spin-transfer Torque Magnetic Memory as a Stochastic Memristive Synapse for Neuromorphic Systems. *IEEE Trans. Biomed. Circuits Syst.* **2015**, *9*, 166−174.

(31) Cao, Y.; Rushforth, A.; Sheng, Y.; Zheng, H.; Wang, K. Tuning a Binary Ferromagnet into a Multistate Synapse with Spin−orbit-torque-induced Plasticity. *Adv. Funct. Mater.* **2019**, *29*, 1808104.

(32) Cao, Y.; Sheng, Y.; Edmonds, K. W.; Ji, Y.; Zheng, H.; Wang, K. Deterministic Magnetization Switching Using Lateral Spin−orbit Torque. *Adv. Mater.* **2020**, *32*, 1907929.

(33) Hayashi, M.; Kim, J.; Yamanouchi, M.; Ohno, H. Quantitative Characterization of the Spin-orbit Torque Using Harmonic Hall Voltage Measurements. *Phys. Rev. B* **2014**, *89*, 144425.

(34) Chen, S.; Yu, J.; Xie, Q.; Zhang, X.; Lin, W.; Liu, L.; Zhou, J.; Shu, X.; Guo, R.; Zhang, Z.; Chen, J. Free Field Electric Switching of Perpendicularly Magnetized Thin Film by Spin Current Gradient. *ACS Appl. Mater. Interfaces* **2019**, *11*, 30446−30452.

(35) Kimata, M.; Chen, H.; Kondou, K.; Sugimoto, S.; Muduli, P. K.; Ikhlas, M.; Omori, Y.; Tomita, T.; MacDonald, A. H.; Nakatsuji, S.; Otani, Y. Magnetic and Magnetic Inverse Spin Hall Effects in a Non-collinear Antiferromagnet. *Nature* **2019**, *565*, 627−630.

(36) Mook, A.; Neumann, R. R.; Johansson, A.; Henk, J.; Mertig, I. Origin of the Magnetic Spin Hall Effect: Spin Current Vorticity in the Fermi Sea. *Phys. Rev. Res.* **2020**, *2*, No. 023065.

(37) Akyol, M.; Alzate, J. G.; Yu, G.; Upadhyaya, P.; Wong, K. L.; Ekicibil, A.; Khalili Amiri, P.; Wang, K. L. Effect of the Oxide Layer on Current-induced Spin-orbit Torques in Hf/CoFeB/MgO and Hf/CoFeB/TaO$_x$ Structures. *Appl. Phys. Lett.* **2015**, *106*, No. 032406.

(38) Cui, B.; Wu, H.; Li, D.; Razavi, S. A.; Wu, D.; Wong, K. L.; Chang, M.; Gao, M.; Zuo, Y.; Xi, L.; Wang, K. L. Field-free Spin−orbit Torque Switching of Perpendicular Magnetization by the Rashba Interface. *ACS Appl. Mater. Interfaces* **2019**, *11*, 39369.

(39) Jin, T.; Law, W. C.; Kumar, D.; Luo, F.; Wong, Q. Y.; Lim, G. J.; Wang, X.; Lew, W. S.; Piramanayagam, S. N. Enhanced Spin−orbit Torque Efficiency in Pt/Co/Ho Heterostructures via Inserting Ho Layer. *APL Mater.* **2020**, *8*, 111111.

(40) Murray, N.; Liao, W. B.; Wang, T. C.; Chang, L. J.; Tsai, L. Z.; Tsai, T. Y.; Lee, S. F.; Pai, C.-F. Field-free Spin-orbit Torque Switching Through Domain Wall Motion. *Phys. Rev. B* **2019**, *100*, 104441.

(41) Xie, Q.; Lin, W.; Sarkar, S.; Shu, X.; Chen, S.; Liu, L.; Zhao, T.; Zhou, C.; Wang, H.; Zhou, J.; Gradečak, S.; Chen, J. Field-free Magnetization Switching Induced by the Unconventional Spin−orbit Torque from WTe2. *APL Mater.* **2021**, *9*, No. 051114.
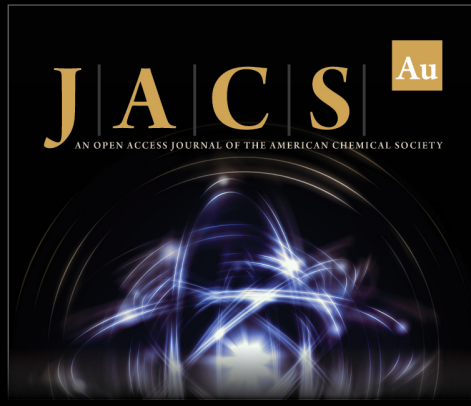
(42) Pai, C. F.; Mann, M.; Tan, A. J.; Beach, G. S. D. Determination of Spin Torque Efficiencies in Heterostructures With Perpendicular Magnetic Anisotropy. *Phys. Rev. B* **2016**, *93*, 144409.

(43) Zhang, R. Q.; Liao, L. Y.; Chen, X. Z.; Xu, T.; Cai, L.; Guo, M. H.; Bai, H.; Sun, L.; Xue, F. H.; Su, J.; Wang, X.; Wan, C. H.; Bai, H.; Song, Y. X.; Chen, R. Y.; Chen, N.; Jiang, W. J.; Kou, X. F.; Cai, J. W.; Wu, H. Q.; Pan, F.; Song, C. Current-induced Magnetization Switching in a CoTb Amorphous Single Layer. *Phys. Rev. B* **2020**, *101*, 214418.

(44) Engel, C.; Goolaup, S.; Luo, F.; Lew, W. S. Quantitative Characterization of Spin-orbit Torques in Pt/Co/Pt/Co/Ta/BTO Heterostructures due to the Magnetization Azimuthal Angle Dependence. *Phys. Rev. B* **2017**, *96*, No. 054407.

(45) Xie, H.; Yuan, J.; Luo, Z.; Yang, Y.; Wu, Y. In-situ Study Of Oxygen Exposure Effect on Spin-orbit Torque in Pt/Co Bilayers in Ultrahigh Vacuum. *Sci. Rep.* **2019**, *9*, 17254.

(46) Du, Y.; Gamou, H.; Takahashi, S.; Karube, S.; Kohda, M.; Nitta, J. Disentanglement of Spin-orbit Torques in Pt/Co Bilayers with the Presence of Spin Hall Effect and Rashba-Edelstein Effect. *Phys. Rev. Appl.* **2020**, *13*, No. 054014.